20-nm skyrmions generated at room-temperature by spin-orbit torques

Jiahao Liu[1,2,3,⊥] , Zidong Wang[1,2,⊥], Teng Xu[1,2], Hengan Zhou[1,2], Le Zhao[1,2], Soong-Guen Je[4,5], Mi-Young Im[4], Liang Fang[3], Wanjun Jiang[1,2,*]

[1]*State Key Laboratory of Low-Dimensional Quantum Physics and Department of Physics, Tsinghua University, Beijing 100084, China*

[2]*Frontier Science Center for Quantum Information, Tsinghua University, Beijing 100084, China*

[3]*Institute for Quantum Information & State Key Laboratory of High Performance Computing, College of Computer, National University of Defense Technology, Changsha 410073, China*

[4]*Center for X-ray Optics, Advanced Light Source, Lawrence Berkeley National Laboratory, Cyclotron Road, Berkeley, CA 94720, USA*

[5]*Department of Physics, Chonnam National University, Gwangju, 61186, Republic of Korea*

Corresponding Author: * Wanjun Jiang, email: jiang_lab@tsinghua.edu.cn

ABSTRACT

The discovery of magnetic skyrmions provides a promising pathway for developing functional spintronic memory and logic devices. Towards the future high-density memory application,

nanoscale skyrmions with miniaturized diameters, ideally down to 20 nm are required. Using an X-ray magnetic circular dichroism (XMCD) transmission microscopy, nanoscale skyrmions are observed in the Pt/Co/Ir multilayer at room temperature. In particular, small skyrmions with a minimum diameter of 20 nm could be generated by the current-induced spin-orbit torques. Through implementing material specific parameters, the dynamic process of skyrmion generation is further investigated by performing micromagnetic simulations. According to the simulation results, we find that both the tube-like Néel-type skyrmions and the bobber-like Néel-type skyrmions can be electrically generated. In particular, the size of the bobber-like Néel-type skyrmions can be effectively reduced by the spin-orbit torques. Our findings could be important for understanding the formation dynamics of nanoscale Néel-type skyrmions, and for promoting nanoscale skyrmionic memory and logic devices.

KEYWORDS skyrmion, multilayers, magnetic bobber, spin-orbit torque, spintronics.

INTRODUCTION

Magnetic skyrmions are considered to be one of the ideal memory cells for spintronic devices due to the advantages of topological protection, high stability, and low energy consumption[1-13]. Since the original theoretical prediction[14, 15], Bloch-type skyrmions were firstly observed in B20-type compounds (such as FeGe[16], FeCoSi[17], MnFeGe[18] and MnSi[19-26]), which however, mainly exist at low temperature. These materials exhibit a non-centrosymmetric lattice structure, in which the accompanied bulk Dzyaloshinskii-Moriya interaction (b-DMI) is responsible for the formation of Bloch-type skyrmions. Meanwhile, Néel-type skyrmions[27, 28]

stabilized by the interfacial DMI (i-DMI) have been found in the inversion-asymmetric heavy metal/ferromagnet (HM/FM) films, such as Pt/CoFe/MgO[29, 30], Pt/Co/Ni/Co/TaN[31] and Pt/Co/AlO_{x}[32]. Furthermore, a strong i-DMI have been identified in magnetic multilayers made of HM/FM bilayers, which leads to the formation of Néel-type skyrmions at room temperature[33, 34]. For examples, Néel-type skyrmions were identified in Ta/CoFeB/TaOx, Pt/Co/Ta and Pt/CoFeB/MgO multilayers, together with their intriguing spin-torque-driven dynamics[35-37]. In particular, Néel-type skyrmions below 100 nm in diameter are observed at room temperature in Ir/Co/Pt multilayers [38, 39], Co/Pd multilayer[40], Ir/Fe/Co/Pt multilayer[41, 42], Pt/Co/IrMn multilayer[43] and Pt/SmCo/Ta multilayer[44]. Since the size of skyrmion directly determines the cell size of the skyrmion-based racetrack memory[45-50], the realization of the nanoscale skyrmions could substantially improve the storage density of these devices[25, 51-56].

In this work, we will explore the formation of room-temperature nanoscale Néel-type skyrmions in a multilayer of $[Pt(1.5\ nm)/Co(1\ nm)/Ir(1.5\ nm)]_{15}$ by using an XMCD transmission microscopy, which is made possible by utilizing the current-induced spin-orbit torques (SOTs). Following the increased current densities, sizes of Néel-type skyrmions decrease accordingly, with the diameter of the smallest skyrmions approaching 20 nm. By performing a layer-resolution micromagnetic simulation, the dynamic process of Néel-type skyrmions formation can be captured. These results reveal the formation of three-dimensional spin textures, including bobber-like and tube-like skyrmions in the present material system.

MATERIALS AND METHODS

Sample preparation and measurement. The sample is grown by using ultrahigh vaccum magnetron sputtering at room temperature with the base pressure of the main chamber at 2×10^{-8} Torr. The sputtering is performed in an argon atmosphere of pressure 3 mTorr, and the sputtering rate is 0.02 nm/s. A 2 nm Ta on 100 nm Si_3N_4 is used as a primer layer, then 15 stacks of Pt(1.5 nm)/Co(1 nm)/Ir(1.5 nm), and finally 2 nm Ta as a protective layer. The device is prepared using electron beam lithography and followed by a lift-off process. The hysteresis loop measurement is obtained by using a vibrating sample magnetometer (VSM). The multilayer is grown on 100 nm thickness Si_3N_4 membrane (Clean SiN, Suzhou) for the XMCD imaging experiment. The XMCD imaging in transmission geometry is done at the Co L_3 edge (778.5 eV) using a full-field transmission soft X-ray microscope (XM-1) at the beamline 6.1.2 at the Advanced Light Source of Lawrence Berkeley National Laboratory.

Micromagnetic simulations. We simulate 15 magnetic layers with i-DMI and dipolar interaction by using a micromagnetic simulation software Mumax3. The current-induced SOT is added to the Landau-Lifshitz-Gilbert (LLG) equation through a custom field. The relax-state solution of the system is calculated after each current pulse. The calculation unit size is $2 \times 2 \times 1$ nm^3, the saturation magnetization is M_s = 1200 kAm^{-1}, the exchange constant is A = 10 pJm^{-1}, the damping coefficient α = 0.01, the perpendicular magnetization anisotropy K_u= 904 kJm^{-3}, the i-DMI intensity D = 1.6 mJm^{-2}[38], and the external magnetic field H_z= 233 mT.

RESULTS

Room-temperature skyrmions in the Pt/Co/Ir multilayer.

The Pt/Co/Ir trilayer could host substantial i-DMI which could be useful for stabilizing nanoscale Néel-type skyrmions[38]. In order to study the current-induced Néel-type skyrmions, a magnetic multilayer of composition and stacking order $[Pt(1.5\ nm)/Co(1\ nm)/Ir(1.5\ nm)]_{15}$ is synthesized, as schematically shown in Fig. 1(a). The out-of-plane magnetic hysteresis loop ($M-H_z$) is measured by using VSM, as shown in Figure 1(b). The shape of the loop is similar to the typical multilayers that host Néel-type skyrmions[35, 41-44]. The saturation magnetization is estimated to be $M_s = ¿$ 1200 kAm^{-1}.

The XMCD images collected at the Co L_3 edge and under magnetic fields are shown on the right panel. For performing XMCD experiment in transmission geometry, multilayers are grown on 100 nm thickness Si_3N_4 membrane. These XMCD imaging experiments are conducted by using a full-field soft X-ray transmission microscopy (XM-1 at the Advanced Light Source, Lawrence Berkeley National Laboratory) with a spatial resolution down to 10 nm[57]. The black color corresponds to the local magnetization pointing downward ($m_z<0$) and the white color corresponds to the local magnetization pointing upward ($m_z>0$). The evolution of magnetic domain configurations as a function of magnetic fields can be found in Figure S1 of Supplementary Materials. Initially, the size of the skyrmions decreases with the increased magnetic field. When the magnetic field is above 299 mT, the average diameter of skyrmions remains as a constant at approximately 58 nm.

20-nm skyrmions induced by current pulses.

In order to probe the SOTs-driven dynamics of skyrmion, we apply current pulses of different durations and current densities to the microstripe device made of multilayer. An optical image of

the device that is fabricated by electron beam lithography is shown in Figure 2(a). Current pulses are applied to the multilayer through the Ta/Pt electrodes on both sides, where the white arrow indicates the positive direction of the current flow. Due to the involvement of heavy metal and the resulting conversion from charge current to spin current, the induced current-induced SOTs can be introduced in the multilayers[58, 59]. Before applying pulse (233 mT), the multilayer is at a coexisting stripe domain-skyrmion state. After applying current pulses of a fixed duration 50 μs with increased current densities (from $0.6\times10^{10}A/m^2$ to $2.4\times10^{10}A/m^2$), the pristine stripe domains are broken (at $0.6\times10^{10}A/m^2$), followed by which a densely packed skyrmion phase is firstly created (at $1.6\times10^{10}A/m^2$), and then the number of skyrmions decreases following the increased amplitudes (from $1.6\times10^{10}A/m^2$ to $2.4\times10^{10}A/m^2$), which can be seen in Figure S2 of Supplementary Materials.

Negative pulses are subsequently applied to reveal the evolution of skyrmion sizes as a function of pulse currents. Figure 2(a) shows an exemplary XMCD image taken after applying a pulse with a current density of $-2.4\times10^{10}A/m^2$. From these data, one can clearly observe the generation of nanoscale skyrmions by the current-induced SOTs. In order to precisely determine the size of skyrmions, we utilize an 360° domain wall model in which the polar angle $\Theta_0(r)$ of the spin rotation, describing the static profile of the Néel-type skyrmion, satisfies the equilibrium equation obtained from the minimization of the energy functional[60]:

$$\nabla^2\Theta_0=\left[\xi^2+\frac{1}{r^2}\right]\sin\Theta_0\cos\Theta_0-\frac{d}{r}\sin^2\Theta_0+h\sin\Theta_0 \quad (1)$$

where $\xi^2 = 2K_u/\mu_0 M_s^2 - 1$, $h = H_z/M_s$, $r = \rho/l_{ex}$ is the reduced polar coordinate and $d = |D|l_{ex}/A$. The exchange length $l_{ex} = \sqrt{2A/\mu_0 M_s^2}$. M_s is the saturation magnetization, μ_0 is the vacuum permeability, A is the exchange constant, K_u is the magnetization anisotropy constant, D is the i-DMI strength, and H_z is the applied magnetic field. An approximate lowest energy solution $\tan\frac{\Theta_0(r)}{2} = \frac{r_{sk}}{r} e^{\xi(r_{sk}-r)}$ is used to fit the skyrmion profile[60]. The fitting results are shown in Figure 2(b). The diameters of the three representative skyrmions are clearly identified as 21 nm, 42 nm and 24 nm, respectively.

Subsequently, we investigate the size distribution of skyrmions under the pulse currents with increased amplitudes. As indicated in Figure 3(a), a gray value threshold is employed to identify the skyrmions in the XMCD images, which were marked in red. The evolution of the estimated skyrmion diameters as a function of the increased current densities is shown in Figure 3(b). As the current density increases, the average skyrmion diameter decreases from 42.5 nm down to 36.5 nm. The distribution of the skyrmion diameters as a function of the current density (from $0.6 \times 10^{10} A/m^2$ to $2.4 \times 10^{10} A/m^2$) is shown in Figure 3(c).

For most of skyrmions, the average diameters decrease with the increased current densities. We, however, find that the size of few skyrmions remain unchanged. Shown in Figure 4(a) is an example, which is from a selected area of Figure 3(c). As the current density increases, one skyrmion on the upper-left corner shrinks in size (marked in yellow circle), while the size of the other two skyrmions on the right remain the same.

DISCUSSION AND CONCLUSION

Micromagnetic simulations.

The underlying physics behind these different responses to the current-induced SOT can be capture by performing the layer-resolved micromagnetic simulations, which is done by using LLG equation[61] with the SOT terms[62]:

$$\dot{m} = -\gamma\, m \times [H_{eff} + \tau_{dam}(m \times p) + \tau_{fie}\, p] + \alpha\, \dot{m} \times m \tag{2}$$

where γ is the gyromagnetic ratio, α is the damping coefficient, m is the normalized magnetization vector, $\dot{m}$ is the time derivative of m. $H_{eff} = \frac{-1}{\mu_0 M_s}\frac{dE}{dm}$ is the effective field where the energy E is given by $E = E_{DMI} + E_{exch} + E_{demag} + E_{aniso} + E_{Zee}$. Here τ_{dam} and τ_{fie} are the amplitudes of the damping-like torque and field-like torque, respectively. In the typical SOT experiment, a damping-like torque $\tau_{dam} = \frac{\hbar\, \theta_{SH}\, J_c}{2\, e\, \mu_0 M_s\, d}$ plays a major role, where $\hbar$ is the reduced Planck constant, J_c is the current density flowing in the heavy metal layer, e is the elementary charge, and d is the thickness of the ferromagnetic layer. For a heavy metal/ferromagnet bilayer, the current pulse is applied in the $\hat{x}$ direction, the spin polarization vector is given by $p = sign(\theta_{SH})\, \hat{j} \times \hat{n} = -\hat{y}$ (surface normal $\hat{n} = \hat{z}$, and spin Hall angle $\theta_{SH} > 0$).

We consider the Neumann boundary conditions, and the i-DMI energy is given by[63]

$$E_{DMI} = D[m_z(\nabla \cdot m) - (m \cdot \nabla) m_z] \tag{3}$$

where D is the i-DMI strength. The i-DMI contribution can be obtained by

$$H_{DMI} = -\frac{1}{\mu_0 M_s}\frac{\mathrm{d}\, E_{DMI}}{\mathrm{d}\, m} = \frac{-2\, D}{\mu_0 M_s}[(\nabla \cdot m)\hat{z} - \nabla m_z] \tag{4}$$

Due to the strong i-DMI in the $[Pt|Co|Ir]_{15}$ multilayer, compact skyrmions in each layer exhibit the same Néel-type chirality as can be seen from Figure 4(b) and (c).

In the thickness dependent simulations, a mixed phase between the stripe domain and isolated skyrmion is introduced at 223 mT. Figure 4(b) shows the simulation results of two individual Néel-type skyrmions from a selected area. The color from blue to red indicates the change of the z-component of magnetization (m_z) from 1 to 0, while the cones represent the magnetization direction. As the figure shows that the skyrmion on the left (marked in yellow circle) gradually shrinks in size as the current density increases. But the size and shape of the other skyrmion remains the same. These simulation results are consistent with the experimental observations shown in Figure 4(a).

Experimentally, the 15 magnetic layers are coupled through the interlayer dipolar interaction[64]. In competition with the i-DMI[65], the system may host two different types of skyrmions (hybridized skyrmions are just examples), as shown in Figure 4(c). One is the compact skyrmions existing across all magnetic layers and form tube-like skyrmions (the right skyrmion in the Figure 4(c)). The other one is the skyrmions that only exist in part of the magnetic layers, as shown in left skyrmion in Figure 4(c). Note that the latter spin texture is similar to chiral bobber, which was recently predicted by theory[66] and experimentally observed below room temperature in materials with b-DMI, such as B20-type alloys[67, 68] and $Cu_2OSeO_{3[69]}$. A chiral bobber is composed of a Bloch-point singularity and a skyrmion tube, which could be useful for enabling reliable skyrmionic device. In line with the chiral Bloch-type bobber in bulk magnets[68, 70, 71], the left skyrmion in Figure 4(c) is stable in multilayer film

with i-DMI, which can be useful for enabling reliable skyrmionic device at room temperature track memory. In the following paper, we use the term bobber-like skyrmion to refer to this object.

A bobber-like skyrmion contains different sizes of layer-dependent skyrmions in the multilayer film, where the skyrmions at the lower layers are smaller than at the upper layer. As a consequence, the cores of the skyrmions in different layers are subjected to different damping-like torques $\tau_{dam} m_z \hat{x}$, and are slightly offset. As the bobber-like skyrmion is shifted slightly by the damping-like torque $\tau_{dam} m_z \hat{x}$, the local field of the interlayer dipole coupling at $\hat{z}$ direction $H_{dipole_z} = \frac{2\,\mathrm{M_s}}{4\pi R^3} m_{i_z} \hat{z}$ of the bobber-like skyrmions at upper layer to the core of the skyrmion at lower layer is weaken (R is the layer-to-layer distance and m_i is the normalized magnetic moment of the adjacent upper layer). As a result, the bobber-like skyrmion is less bounded by the interlayer dipole coupling, in comparison with the tube-like skyrmions, which gradually shrinks in size upon the application of current-induced SOTs.

In a conclusion, by using element resolved XMCD imaging technique, we have observed the generation of room-temperature magnetic skyrmions with an average diameter of 58 nm experimentally in the Pt/Co/Ir multilayer. The skyrmions with minimum diameter of ~ 20 nm are further obtained by applying current pulses. Through performing a layer-resolved micromagnetic simulation, we have revealled that both bobber-like and tube-like skyrmions may exist stably in the multilayer. In particular, the bobber-like skyrmions are susceptible to the current-induced SOT, which shrink in size upon the application of currents. This work may provide a method for

the generation of nanoscale skyrmions in multilayer, which could be important for the continuous exploration of intriguing topological physics, and the skyrmion-based racetrack memory.

SUPPORTING INFORMATION

The following file is available free of charge:

Supplementary figures S1-S2 (PDF)

CONFLICT OF INTEREST

The authors declare that they have no conflict of interest.

ACKNOWLEDGMENTS

This work was supported by the Basic Science Center Project of NSFC (Grant No. 51788104), National Key R&D Program of China (Grant Nos. 2017YFA020620, 2018YFB1003304), the National Natural Science Foundation of China (Grant No. 11774194, 51831005, 1181101082, 11804182, 61832007), Beijing Natural Science Foundation (Grant No. Z190009), and the Beijing Advanced Innovation Center for Future Chip (ICFC). Works at the ALS were supported by U.S. Department of Energy (DE-AC02-05CH11231).

AUTHOR CONTRIBUTIONS

[⊥]These authors contributed equally to this work. W.J. conceived the idea. Z.W., T.X., H.Z. and L.Z. prepared the device. Z.W. made the VSM measurements. Z.W., S.J., M.I. and W.J. performed the soft X-ray microscopy imaging experiments. J.L. performed the data analysis, skyrmion profile fittings and micromagnetic simulations. W.J. wrote the manuscript with inputs from all authors.

REFERENCES

[1] A.H. Bogdanov, A. , Thermodynamically stable magnetic vortex states in magnetic crystals, J Mag Mag Mater, 138 (1994) 225-269.
[2] A.N. Bogdanov, U.K. Rossler, Chiral symmetry breaking in magnetic thin films and multilayers, Phys Rev Lett, 87 (2001) 037203.
[3] A. Fert, N. Reyren, V. Cros, Magnetic skyrmions: advances in physics and potential applications, Nature Reviews Materials, 2 (2017) 17031.
[4] X.Z. Yu, Y. Onose, N. Kanazawa, J.H. Park, J.H. Han, Y. Matsui, N. Nagaosa, Y. Tokura, Real-space observation of a two-dimensional skyrmion crystal, Nature, 465 (2010) 901-904.
[5] N. Nagaosa, Y. Tokura, Topological properties and dynamics of magnetic skyrmions, Nature Nanotechnology, 8 (2013) 899-911.
[6] W. Koshibae, Y. Kaneko, J. Iwasaki, M. Kawasaki, Y. Tokura, N. Nagaosa, Memory functions of magnetic skyrmions, Japanese Journal of Applied Physics, 54 (2015) 053001.
[7] G. Chen, A. Mascaraque, A.T. N'Diaye, A.K. Schmid, Room temperature skyrmion ground state stabilized through interlayer exchange coupling, Applied Physics Letters, 106 (2015) 556.
[8] H.B. Braun, Topological effects in nanomagnetism: from superparamagnetism to chiral quantum solitons, Advances in Physics, 61 (2012) 1-116.
[9] F. Buettner, C. Moutafis, M. Schneider, B. Krueger, C.M. Guenther, J. Geilhufe, C.V. Schmising, J. Mohanty, B. Pfau, S. Schaffert, A. Bisig, M. Foerster, T. Schulz, C.A.F. Vaz, J.H. Franken, H.J.M. Swagten, M. Klaui, S. Eisebitt, Dynamics and inertia of skyrmionic spin structures, Nat. Phys., 11 (2015) 225-228.
[10] S.H. Yang, R. Naaman, Y. Paltiel, S.S.P. Parkin, Chiral spintronics, Nature Reviews Physics, 3 (2021) 328-343.
[11] B. Gobel, I. Mertig, O.A. Tretiakov, Beyond skyrmions: Review and perspectives of alternative magnetic quasiparticles, Physics Reports-Review Section of Physics Letters, 895 (2021) 1-28.
[12] C. Back, V. Cros, H. Ebert, K. Everschor-Sitte, A. Fert, M. Garst, T. Ma, S. Mankovsky, T.L. Monchesky, M. Mostovoy, N. Nagaosa, S.S.P. Parkin, C. Pfleiderer, N. Reyren, A. Rosch, Y. Taguchi, Y. Tokura, K. von Bergmann, J. Zang, The 2020 skyrmionics roadmap, Journal of Physics D: Applied Physics, 53 (2020) 363001.
[13] K. Everschor-Sitte, J. Masell, R.M. Reeve, M. Klaui, Perspective: Magnetic skyrmions-Overview of recent progress in an active research field, Journal of Applied Physics, 124 (2018) 240901.

[14] T.H.R. Skyrme, Particle States of a Quantized Meson Field, P Roy Soc A-Math Phy, 262 (1961) 237-245.
[15] N.Y. Bogdanov, D. A, Thermodynamically stable “vortices” in magnetically ordered crystals: the mixed state of magnets, Sov. Phys. JETP, 68 (1989) 101–103.
[16] S.X. Huang, C.L. Chien, Extended Skyrmion phase in epitaxial FeGe(111) thin films, Phys Rev Lett, 108 (2012) 267201.
[17] X.Z. Yu, Y. Onose, N. Kanazawa, J.H. Park, J.H. Han, Y. Matsui, N. Nagaosa, Y. Tokura, Real-space observation of a two-dimensional skyrmion crystal, Nature, 465 (2010) 901-904.
[18] K. Shibata, X.Z. Yu, T. Hara, D. Morikawa, N. Kanazawa, K. Kimoto, S. Ishiwata, Y. Matsui, Y. Tokura, Towards control of the size and helicity of skyrmions in helimagnetic alloys by spin-orbit coupling, Nat Nanotechnol, 8 (2013) 723-728.
[19] R. Ritz, M. Halder, M. Wagner, C. Franz, A. Bauer, C. Pfleiderer, Formation of a topological non-Fermi liquid in MnSi, Nature, 497 (2013) 231-234.
[20] A. Neubauer, C. Pfleiderer, B. Binz, A. Rosch, R. Ritz, P.G. Niklowitz, P. Boni, Topological Hall effect in the A phase of MnSi, Phys Rev Lett, 102 (2009) 186602.
[21] C. Pappas, E. Lelievre-Berna, P. Falus, P.M. Bentley, E. Moskvin, S. Grigoriev, P. Fouquet, B. Farago, Chiral paramagnetic skyrmion-like phase in MnSi, Phys Rev Lett, 102 (2009) 197202.
[22] A. Tonomura, X. Yu, K. Yanagisawa, T. Matsuda, Y. Onose, N. Kanazawa, H.S. Park, Y. Tokura, Real-space observation of skyrmion lattice in helimagnet MnSi thin samples, Nano Lett, 12 (2012) 1673-1677.
[23] X.Z. Yu, J.P. DeGrave, Y. Hara, T. Hara, S. Jin, Y. Tokura, Observation of the Magnetic Skyrmion Lattice in a MnSi Nanowire by Lorentz TEM, Nano Letters, 13 (2013) 3755-3759.
[24] H.F. Du, J.P. DeGrave, F. Xue, D. Liang, W. Ning, J.Y. Yang, M.L. Tian, Y.H. Zhang, S. Jin, Highly Stable Skyrmion State in Helimagnetic MnSi Nanowires, Nano Letters, 14 (2014) 2026-2032.
[25] F. Jonietz, S. Muhlbauer, C. Pfleiderer, A. Neubauer, W. Munzer, A. Bauer, T. Adams, R. Georgii, P. Boni, R.A. Duine, K. Everschor, M. Garst, A. Rosch, Spin Transfer Torques in MnSi at Ultralow Current Densities, Science, 330 (2010) 1648-1651.
[26] J. Kindervater, I. Stasinopoulos, A. Bauer, F.X. Haslbeck, F. Rucker, A. Chacon, S. Muhlbauer, C. Franz, M. Garst, D. Grundler, C. Pfleiderer, Weak Crystallization of Fluctuating Skyrmion Textures in MnSi, Physical Review X, 9 (2019) 041059.
[27] S. Heinze, K. von Bergmann, M. Menzel, J. Brede, A. Kubetzka, R. Wiesendanger, G. Bihlmayer, S. Blugel, Spontaneous atomic-scale magnetic skyrmion lattice in two dimensions, Nat. Phys., 7 (2011) 713-718.
[28] N. Romming, C. Hanneken, M. Menzel, J.E. Bickel, B. Wolter, K. von Bergmann, A. Kubetzka, R. Wiesendanger, Writing and Deleting Single Magnetic Skyrmions, Science, 341 (2013) 636-639.
[29] S. Emori, U. Bauer, S.M. Ahn, E. Martinez, G.S. Beach, Current-driven dynamics of chiral ferromagnetic domain walls, Nat Mater, 12 (2013) 611–616.
[30] O. Boulle, J. Vogel, H.X. Yang, S. Pizzini, D.D. Chaves, A. Locatelli, T.O. Mentes, A. Sala, L.D. Buda-Prejbeanu, O. Klein, M. Belmeguenai, Y. Roussigne, A. Stashkevich, S.M. Cherif, L. Aballe, M. Foerster, M. Chshiev, S. Auffret, I.M. Miron, G. Gaudin, Room-temperature chiral magnetic skyrmions in ultrathin magnetic nanostructures, Nature Nanotechnology, 11 (2016) 449-454.

[31] M.C. DeRosa, C. Monreal, M. Schnitzer, R. Walsh, Y. Sultan, Nanotechnology in fertilizers, Nat Nanotechnol, 5 (2010) 91.
[32] S. Pizzini, J. Vogel, S. Rohart, L.D. Buda-Prejbeanu, E. Jue, O. Boulle, I.M. Miron, C.K. Safeer, S. Auffret, G. Gaudin, A. Thiaville, Chirality-Induced asymmetric magnetic nucleation in Pt/Co/AlOx ultrathin microstructures, Phys Rev Lett, 113 (2014) 047203.
[33] W. Jiang, G. Chen, K. Liu, J. Zang, S.G.E. te Velthuis, A. Hoffmann, Skyrmions in magnetic multilayers, Physics Reports, 704 (2017) 1-49.
[34] B. Dupe, G. Bihlmayer, M. Bottcher, S. Blugel, S. Heinze, Engineering skyrmions in transition-metal multilayers for spintronics, Nature Communications, 7 (2016) 11779.
[35] S. Woo, K. Litzius, B. Kruger, M.Y. Im, L. Caretta, K. Richter, M. Mann, A. Krone, R.M. Reeve, M. Weigand, P. Agrawal, I. Lemesh, M.A. Mawass, P. Fischer, M. Klaui, G.S. Beach, Observation of room-temperature magnetic skyrmions and their current-driven dynamics in ultrathin metallic ferromagnets, Nat Mater, 15 (2016) 501-506.
[36] W. Jiang, P. Upadhyaya, W. Zhang, G. Yu, M.B. Jungfleisch, F.Y. Fradin, J.E. Pearson, Y. Tserkovnyak, K.L. Wang, O. Heinonen, S.G. te Velthuis, A. Hoffmann, Magnetism. Blowing magnetic skyrmion bubbles, Science, 349 (2015) 283-286.
[37] W. Li, I. Bykova, S. Zhang, G. Yu, R. Tomasello, M. Carpentieri, Y. Liu, Y. Guang, J. Grafe, M. Weigand, D.M. Burn, G. van der Laan, T. Hesjedal, Z. Yan, J. Feng, C. Wan, J. Wei, X. Wang, X. Zhang, H. Xu, C. Guo, H. Wei, G. Finocchio, X. Han, G. Schutz, Anatomy of Skyrmionic Textures in Magnetic Multilayers, Adv Mater, 31 (2019) e1807683.
[38] C. Moreau-Luchaire, S.C. Mouta, N. Reyren, J. Sampaio, C.A. Vaz, N. Van Horne, K. Bouzehouane, K. Garcia, C. Deranlot, P. Warnicke, P. Wohlhuter, J.M. George, M. Weigand, J. Raabe, V. Cros, A. Fert, Additive interfacial chiral interaction in multilayers for stabilization of small individual skyrmions at room temperature, Nat Nanotechnol, 11 (2016) 444-448.
[39] W. Legrand, D. Maccariello, N. Reyren, K. Garcia, C. Moutafis, C. Moreau-Luchaire, S. Coffin, K. Bouzehouane, V. Cros, A. Fert, Room-Temperature Current-Induced Generation and Motion of sub-100 nm Skyrmions, Nano Letters, 17 (2017) 2703-2712.
[40] S.D. Pollard, J.A. Garlow, J. Yu, Z. Wang, Y. Zhu, H. Yang, Observation of stable Neel skyrmions in cobalt/palladium multilayers with Lorentz transmission electron microscopy, Nat Commun, 8 (2017) 14761.
[41] A. Soumyanarayanan, M. Raju, A.L. Gonzalez Oyarce, A.K.C. Tan, M.Y. Im, A.P. Petrovic, P. Ho, K.H. Khoo, M. Tran, C.K. Gan, F. Ernult, C. Panagopoulos, Tunable room-temperature magnetic skyrmions in Ir/Fe/Co/Pt multilayers, Nat Mater, 16 (2017) 898-904.
[42] M. Raju, A. Yagil, A. Soumyanarayanan, A.K.C. Tan, A. Almoalem, F.S. Ma, O.M. Auslaender, C. Panagopoulos, The evolution of skyrmions in Ir/Fe/Co/Pt multilayers and their topological Hall signature, Nature Communications, 10 (2019) 696.
[43] Y. Guang, I. Bykova, Y. Liu, G. Yu, E. Goering, M. Weigand, J. Grafe, S.K. Kim, J. Zhang, H. Zhang, Z. Yan, C. Wan, J. Feng, X. Wang, C. Guo, H. Wei, Y. Peng, Y. Tserkovnyak, X. Han, G. Schutz, Creating zero-field skyrmions in exchange-biased multilayers through X-ray illumination, Nat Commun, 11 (2020) 949.
[44] H.A. Zhou, J.H. Liu, Z.D. Wang, Q.H. Zhang, T. Xu, Y.Q. Dong, L. Zhao, S.G. Je, M.Y. Im, K. Xu, J. Zhu, W.J. Jiang, Rare-Earth Permanent Magnet SmCo5 for Chiral Interfacial Spin-Orbitronics, Advanced Functional Materials, (2021) 2104426.
[45] A. Fert, V. Cros, J. Sampaio, Skyrmions on the track, Nat Nanotechnol, 8 (2013) 152-156.

[46] S.S.P. Parkin, M. Hayashi, L. Thomas, Magnetic domain-wall racetrack memory, Science, 320 (2008) 190-194.
[47] J. Iwasaki, M. Mochizuki, N. Nagaosa, Current-induced skyrmion dynamics in constricted geometries, Nat Nanotechnol, 8 (2013) 742-747.
[48] J. Sampaio, V. Cros, S. Rohart, A. Thiaville, A. Fert, Nucleation, stability and current-induced motion of isolated magnetic skyrmions in nanostructures, Nat Nanotechnol, 8 (2013) 839-844.
[49] J.J. Ding, X.F. Yang, T. Zhu, Manipulating current induced motion of magnetic skyrmions in the magnetic nanotrack, Journal of Physics D-Applied Physics, 48 (2015) 115004.
[50] R. Juge, K. Bairagi, K.G. Rana, J. Vogel, M. Sall, D. Mailly, V.T. Pham, Q. Zhang, N. Sisodia, M. Foerster, L. Aballe, M. Belmeguenai, Y. Roussigne, S. Auffret, L.D. Buda-Prejbeanu, G. Gaudin, D. Ravelosona, O. Boulle, Helium Ions Put Magnetic Skyrmions on the Track, Nano Letters, 21 (2021) 2989-2996.
[51] T. Schulz, R. Ritz, A. Bauer, M. Halder, M. Wagner, C. Franz, C. Pfleiderer, K. Everschor, M. Garst, A. Rosch, Emergent electrodynamics of skyrmions in a chiral magnet, Nat. Phys., 8 (2012) 301-304.
[52] X.Z. Yu, N. Kanazawa, W.Z. Zhang, T. Nagai, T. Hara, K. Kimoto, Y. Matsui, Y. Onose, Y. Tokura, Skyrmion flow near room temperature in an ultralow current density, Nature Communications, 3 (2012) 988
[53] X.Y. Zhang, W.L. Cai, X.C. Zhang, Z.L. Wang, Z. Li, Y. Zhang, K.H. Cao, N. Lei, W. Kang, Y. Zhang, H.M. Yu, Y. Zhou, W.S. Zhao, Skyrmions in Magnetic Tunnel Junctions, Acs Applied Materials & Interfaces, 10 (2018) 16887-16892.
[54] J. Zazvorka, F. Jakobs, D. Heinze, N. Keil, S. Kromin, S. Jaiswal, K. Litzius, G. Jakob, P. Virnau, D. Pinna, K. Everschor-Sitte, L. Rozsa, A. Donges, U. Nowak, M. Klaui, Thermal skyrmion diffusion used in a reshuffler device, Nat Nanotechnol, 14 (2019) 658-661.
[55] S. Li, W. Kang, X.C. Zhang, T.X. Nie, Y. Zhou, K.L. Wang, W.S. Zhao, Magnetic skyrmions for unconventional computing, Materials Horizons, 8 (2021) 854-868.
[56] W. Kang, S. Li, X. Chen, D. Zhu, X. Zhang, N. Lei, W. Zhao, Unconventional applications of skyrmions, in: G. Finocchio, C. Panagopoulos (Eds.) Magnetic Skyrmions and Their Applications, Woodhead Publishing 2021, pp. 393-416.
[57] Z. Wang, M. Guo, H.-A. Zhou, L. Zhao, T. Xu, R. Tomasello, H. Bai, Y. Dong, S.-G. Je, W. Chao, H.-S. Han, S. Lee, K.-S. Lee, Y. Yao, W. Han, C. Song, H. Wu, M. Carpentieri, G. Finocchio, M.-Y. Im, S.-Z. Lin, W. Jiang, Thermal generation, manipulation and thermoelectric detection of skyrmions, Nature Electronics, 3 (2020) 672-679.
[58] J. Sinova, S.O. Valenzuela, J. Wunderlich, C.H. Back, T. Jungwirth, Spin Hall effects, Reviews of Modern Physics, 87 (2015) 1213-1259.
[59] G.Q. Yu, P. Upadhyaya, X. Li, W.Y. Li, S.K. Kim, Y.B. Fan, K.L. Wong, Y. Tserkovnyak, P.K. Amiri, K.L. Wang, Room-Temperature Creation and Spin Orbit Torque Manipulation of Skyrmions in Thin Films with Engineered Asymmetry, Nano Letters, 16 (2016) 1981-1988.
[60] R. Tomasello, K.Y. Guslienko, M. Ricci, A. Giordano, J. Barker, M. Carpentieri, O. Chubykalo-Fesenko, G. Finocchio, Origin of temperature and field dependence of magnetic skyrmion size in ultrathin nanodots, Physical Review B, 97 (2018) 060402(R).
[61] L.D.L. Landau, E. M., On the theory of the dispersion of magnetic permeability in ferromagnetic bodies, Phys. Z. Sowjetunion, 8 153-169.

[62] F. Buttner, I. Lemesh, M. Schneider, B. Pfau, C.M. Gunther, P. Hessing, J. Geilhufe, L. Caretta, D. Engel, B. Kruger, J. Viefhaus, S. Eisebitt, G.S.D. Beach, Field-free deterministic ultrafast creation of magnetic skyrmions by spin-orbit torques, Nat Nanotechnol, 12 (2017) 1040-1044.
[63] S. Rohart, A. Thiaville, Skyrmion confinement in ultrathin film nanostructures in the presence of Dzyaloshinskii-Moriya interaction, Physical Review B, 88 (2013) 184422.
[64] R. Lo Conte, A.K. Nandy, G. Chen, A.L.F. Cauduro, A. Maity, C. Ophus, Z.J. Chen, A.T. N'Diaye, K. Liu, A.K. Schmid, R. Wiesendanger, Tuning the Properties of Zero-Field Room Temperature Ferromagnetic Skyrmions by Interlayer Exchange Coupling, Nano Letters, 20 (2020) 4739-4747.
[65] A. Bernand-Mantel, C.B. Muratov, T.M. Simon, Unraveling the role of dipolar versus Dzyaloshinskii-Moriya interactions in stabilizing compact magnetic skyrmions, Physical Review B, 101 (2020) 045416.
[66] F.N. Rybakov, A.B. Borisov, S. Blugel, N.S. Kiselev, New Type of Stable Particlelike States in Chiral Magnets, Physical Review Letters, 115 (2015) 117201.
[67] A.S. Ahmed, J. Rowland, B.D. Esser, S.R. Dunsiger, D.W. McComb, M. Randeria, R.K. Kawakami, Chiral bobbers and skyrmions in epitaxial FeGe/Si(111) films, Physical Review Materials, 2 (2018) 041401(R).
[68] F. Zheng, F.N. Rybakov, A.B. Borisov, D. Song, S. Wang, Z.A. Li, H. Du, N.S. Kiselev, J. Caron, A. Kovacs, M. Tian, Y. Zhang, S. Blugel, R.E. Dunin-Borkowski, Experimental observation of chiral magnetic bobbers in B20-type FeGe, Nat Nanotechnol, 13 (2018) 451-455.
[69] K. Ran, Y. Liu, Y. Guang, D.M. Burn, G. van der Laan, T. Hesjedal, H. Du, G. Yu, S. Zhang, Creation of a Chiral Bobber Lattice in Helimagnet-Multilayer Heterostructures, Phys Rev Lett, 126 (2021) 017204.
[70] J. Zhu, Y.D. Wu, Q.Y. Hu, L.Y. Kong, J. Tang, M.L. Tian, H.F. Du, Current-driven transformations of a skyrmion tube and a bobber in stepped nanostructures of chiral magnets, Sci. China-Phys. Mech. Astron., 64 (2021) 6.
[71] Z.Z. Gong, J. Tang, S.S. Pershoguba, Z.K. Xie, R. Sun, Y. Li, X. Yang, J.A. Liu, W. Zhang, X.Q. Zhang, W. He, H.F. Du, J.D. Zang, Z.H. Cheng, Current-induced dynamics and tunable spectra of a magnetic chiral bobber, Physical Review B, 104 (2021) L100412.

FIGURES

Figure 1. Magnetic properties of Pt/Co/Ir multilayer. (a) Schematic illustration of the $[Pt/Co/Ir]_{15}$ multilayer film. A 2 nm-thick Ta layer is sputtered on the substrate as a primer layer and another 2 nm-thick Ta layer on the top is a protective layer. (b) The magnetic hysteresis loop of the

multilayer. The magnetic domain configurations at the selected magnetic fields were recorded by using a XMCD transmission microscope. Room-temperature skyrmions are observed at ~ ± 300 mT. The scale bar is 1 μm.

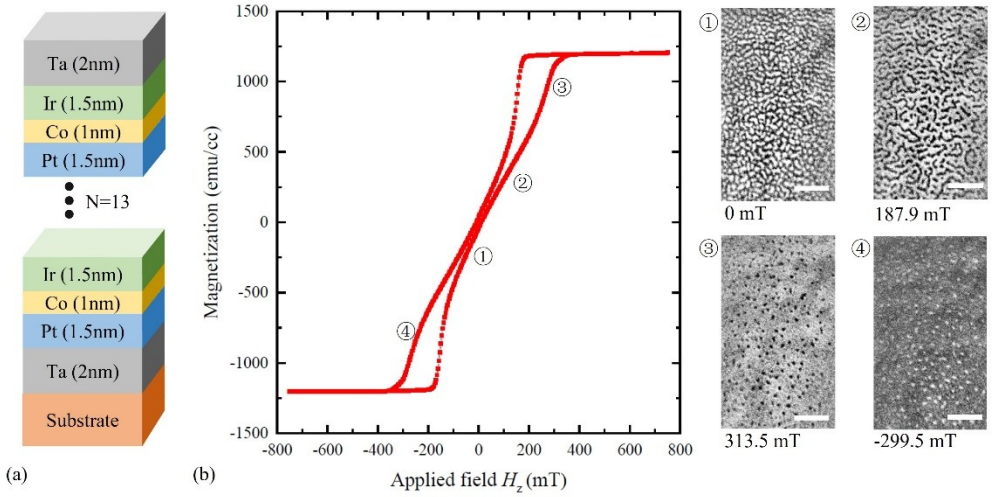

Figure 2. The generation of nanoscale skyrmions by current pulse at room temperature. (a) An optical image of the device. The white arrow indicates the direction of the current pulse. The

scale bar is 20 μm. (b) XMCD images taken after a pulse with a current density of $-2.4\times10^{10}\,A/m^2$) and a width of 50 μs, at a perpendicular magnetic field of $H_z=-223\,mT$. The scale bar is 200 nm. (c) The profile of three selected skyrmions which are marked by red circles. The black circles are the experimental data extracted from the XCMD images, and the red line is the fitted profile. The fitting diameters of are the three skyrmions are 21 nm, 42 nm, and 24 nm, respectively.

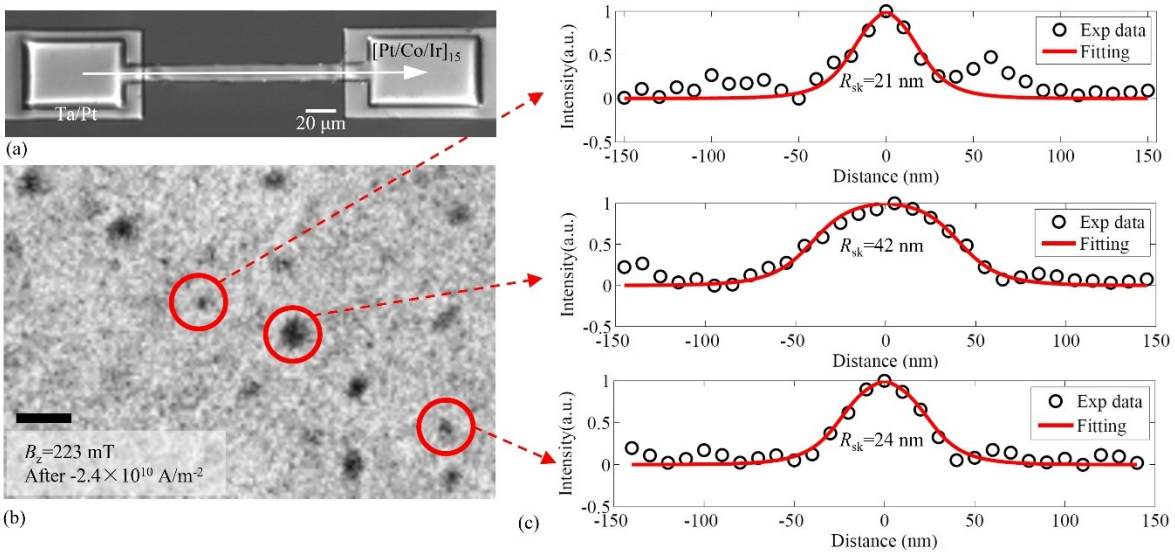

Figure 3. The size distribution of skyrmions under pulses with various current densities. (a) A gray threshold method is used to identify skyrmions (marked in red). The scale bar is 500 nm. (b)

The average diameter of skyrmions as a function of the current density. (c) The statistics of the skyrmion diameters under pulses with various current densities. The scale bar is 500 nm.

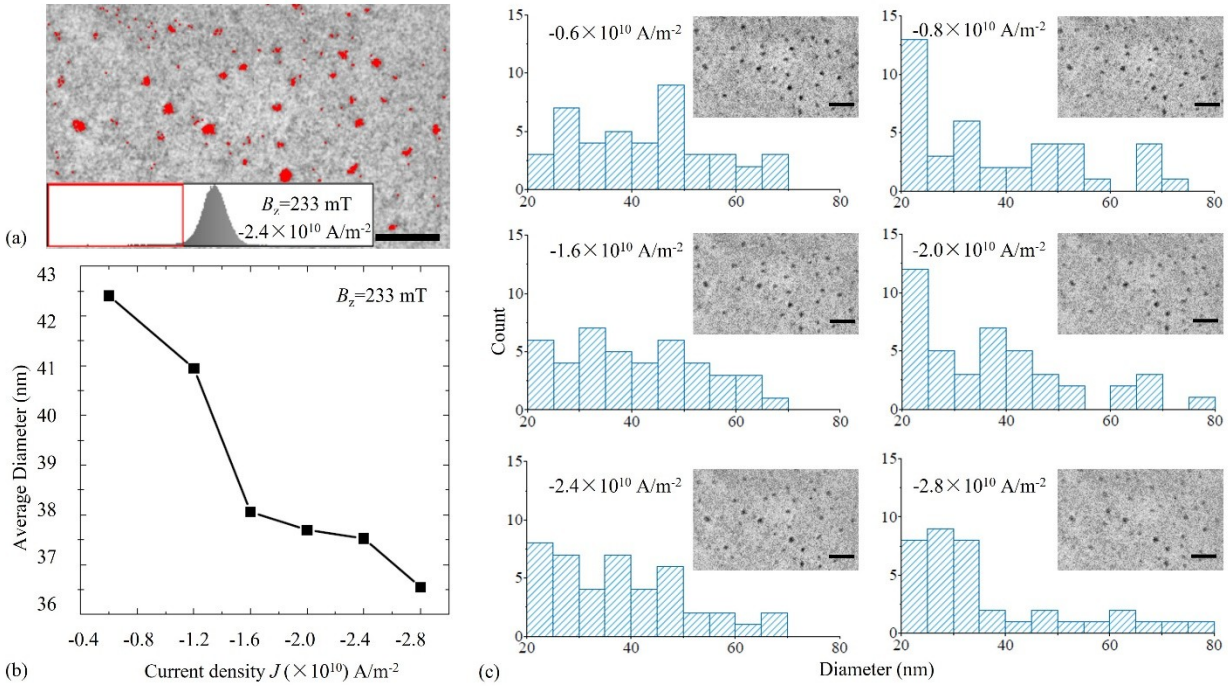

Figure 4. Micromagnetic simulation of the dynamic response of skyrmion produced by current-induced SOT. (a) A selected area with three skyrmions from the XMCD images in Figure 3 (c) under the increased amplitude of the current pulse. The skyrmion that is circled by the yellow

circle on the upper-left corner, shrinks its size, while the size of rest two skyrmions on the right, remain nearly unchanged. The scale bar is 200 nm. (b) The corresponding micromagnetic simulation under increased current density, which produces consistent behavior as experimental observations. The color from blue to red indicates m_z from 1 to 0 while the cones represent the magnetization direction. (c) 3D-view of the two types of skyrmions. A bobber-like skyrmion (left) and a tube-like skyrmion (right) can be identified.